DVH analysis for brachytherapy plaques and proton beam during intraocular tumor treatment using 3D film dosimetry

Taha Eidi (taha.eidi64@gmail.com)
Shahid Beheshti University
Seyed Mahmoud Reza Aghamiri
Shahid Beheshti University
Hamid Reza Baghani
Hakim Sabzevari University

Research Article

Keywords: Intraocular tumor, Proton beam, 125I COMS plaque, 106Ru CGD plaque, Dosimetric characteristics, Film dosimetry

Posted Date: January 16th, 2023

DOI: https://doi.org/10.21203/rs.3.rs-2432913/v1

Abstract

Proton therapy and plaque-based brachytherapy are considered efficient radiotherapy modalities for intraocular tumor irradiation. The current study aims to measure and compare the dosimetric features of these methods through a film dosimetry approach inside an eyeball phantom.

A 3D-printed PLA (polylactic acid)-based eyeball phantom was applied for phantom irradiation. For brachytherapy, COMS and CGD plaques respectively containing the ^{125}I and ^{106}Ru radioactive sources were employed. Proton irradiation was performed using the clinical beamline of the CNAO oncological hadron therapy center. PDD (percentage depth dose), transverse dose profile, 2D and 3D dose distribution, as well as DVH (dose volume histogram) data relevant to the tumor volume and surrounding healthy tissues were measured for applied treatment techniques using Gafchromic EBT3 film dosimetry approach and compared together.

A more uniform dose distribution inside the tumor volume was found in the case of the proton beam concerning two other techniques. Furthermore, a proton beam can better spare healthy organs distributed around the tumor region. Besides, COMS plaque can lead to better clinical outcomes concerning CGD plaque.

Viewpoint to the dose uniformity inside the target volume as well as sparing the healthy tissues, proton therapy would be the optimal choice. On the other hand, the photon beam can be preferred to the electron beam if proton therapy facilities are not available. Nevertheless, based on the importance of the healthy organ which should be spared, the COMS or CGD plaque can be selected for radiotherapy.

1. Introduction

Uveal melanoma is considered as one of the malignant intraocular tumors with an annual occurrence rate of one per 100000 people each year [1, 2]. Regarding the invasive and life-threatening nature of this malignant tumor type, effective treatment modalities should be applied when the treatment team decides to conserve the patient's eyeball. Radiotherapy can serve as an effective method for irradiation and local control of intraocular tumors, especially in the case of uveal melanoma [3, 4].

One of the main limitations during the radiotherapy of intraocular tumors is the presence of sensitive organs and healthy tissues such as optic nerve, optic disc, eye lens, retina, etc. which can be distributed at close distances to the intraocular tumor [4–6]. As a result, conventional radiotherapy techniques such as external photon and electron radiotherapy techniques cannot be effectively employed for intraocular tumor irradiation due to the overexposure of such healthy tissues and organs at risk (OARs) [7, 8]. In return, more advanced radiotherapy modalities such as brachytherapy or hadron therapy are better suited for intraocular tumor irradiation, because these techniques can better localize the radiation field to the treatment volume as well as more efficiently spare the surrounding healthy tissues from overexposure [8, 9].

Brachytherapy can be implemented through three different techniques including surface, interstitial, and intra-cavitary ones [10, 11]. For intraocular brachytherapy purposes, the well-adopted technique is surface brachytherapy [10]. The most comment radioactive sources which are used with this technique for intraocular tumor irradiation are Iodine-125 (^{125}I), Palladium-103 (^{103}Pd), and Ruthenium-106 (^{106}Ru) [12, 13]. ^{106}Ru is a beta-emitting radiation source, while ^{125}I and ^{103}Pd are considered gamma-emitter sources. Due to the more limited range of the beta radiation with respect to the gamma one, employing the ^{106}Ru source can reduce the received dose by surrounding and underlying healthy tissues during the brachytherapy of the intraocular tumors [14, 15]. In addition, the treatment staff is also less exposed to radiation when the ^{106}Ru radioactive source is employed for brachytherapy [16, 17]. On the other hand, employing the ^{106}Ru source for deeply distributed intraocular tumors is not appropriate because the limited range of beta particles may cause inadequate coverage of the tumor volume by the intended isodose level. In such situations, the gamma sources such as ^{125}I and ^{103}Pd are preferred due to the more range of photon beam with respect to the beta particles. Therefore, using each type of brachytherapy source (beta or gamma emitter) has its advantages and limitations.

For radiation source holding, positioning, and manipulation during the patient treatment, each of the above-mentioned radioactive sources should be kept within an appropriate applicator which is known as the eye plaque. In the case of ^{106}Ru, the radiation source is not available in the seed form. On the other hand, it would be coated over the inner plaque surface to form a very thin radioactive layer [18, 19]. Although the ^{125}I radioactive material is prepared in the seed form for brachytherapy purposes, it should be also located inside a dedicated eye plaque for intraocular tumor irradiation [15, 16]. One of the most popular plaques for this purpose is the COMS one which ^{125}I seeds are arranged on the inner surface of this plaque based on the size and extension of the tumor which should be irradiated [2, 12, 20].

The alternative option for intraocular tumor irradiation is hadron therapy. This technique is considered a newer modality for uveal melanoma treatment in comparison with the brachytherapy technique. In this regard, a proton beam, Helium ion, or Carbon ion can be applied for tumor irradiation [21–23]. Due to the specific behavior of these charged particle energy loss along the depth, known as the Bragg curve and Bragg peak, one can form a wide homogeneous absorbed dose plateau by combining the relevant Bragg curves to the different beam weights and energies which is known as as the spread-out Bragg peak (SOBP). Formation of the SOBP can effectively help to localize the radiation field inside the treatment volume and extract the OARs from the treatment field [24, 25]. Currently, the proton beam is the most commonly charged particle that is employed for intraocular hadron therapy. In this regard, proton energies which range from 60 MeV to 250 MeV can be used for radiotherapy purposes [6, 22, 26].

Although both techniques, brachytherapy and proton therapy, are well adapted for intraocular tumor treatment, it would be valuable to quantitatively compare the treatment outcomes in terms of 3D dose distribution, dose uniformity inside the target volume, as well as the received dose by the surrounding healthy tissues for both candidate treatment modalities. Accordingly, the current study aims to measure and compare the relevant dose distribution to the ^{125}I and ^{106}Ru-based eye brachytherapy plaques as well

as the proton beam inside an eyeball phantom at the same clinical conditions (tumor size and position inside the eyeball) through the Gafchromic film dosimetry approach and finally demonstrate that employing which technique can lead to more desirable treatment outcomes viewpoint to the clinical radiation oncology physics.

2. Materials And Methods

2.1. Eyeball phantom

A PLA (Polylactic Acid)-based plastic phantom which mimics the geometry of the eyeball was used in the current study. The choice of the PLA as the constructing material was its desirable water equivalency [27, 28], the reference medium for radiation dosimetry purposes. This phantom is composed of two separate parts including a semispherical part that simulates the curvature of the eyeball and a cubic part that comprises the underlying eyeball tissues. The semispherical part is a section of a sphere with a 13 mm radius and its height is equal to 5.1 mm. The aperture of this semispherical part is also equal to 22.3 mm. The cubic part of the phantom has dimensions of 40×40×0.9 mm^3. It should be mentioned that the employed phantom was developed and constructed through a 3D printing procedure. A schematic view of the designed eyeball phantom has been shown in Fig. 1.

Figure 1.

2.2. Film dosimetry

Film dosimetry is one of the most appropriate approaches for radiation dosimetry in clinical practice [29, 30]. In this regard, several films such as radiographic and radiochromic ones have been introduced for film dosimetry purposes. Due to the high dose delivery during the intraocular radiotherapy, the radiochromic films are better suited for such dosimetry purposes, because they would not be saturated up to high doses of as much as 100 Gy [31, 32]. Consequently, the Gafchromic EBT3 film (ISP), a type of radiochromic film, was applied for dosimetry of both proton, ^{125}I, and ^{106}Ru brachytherapy plaques. This film has a symmetric structure which respectively includes 125 μm thickness Mate polyester over-layer, 28 μm thickness active layer, and 125 μm thickness Mate polyester substrate [5, 33]. One of the main features of this Gafchromic film is its very near tissue equivalency which allows the user to measure the absorbed dose with good accuracy. For ^{125}I and ^{106}Ru plaque dose measurements, the Gafchromic EBT3 films were calibrated using a Co-60 machine at the dose range of 0.5–55 Gy. On the other hand, the conducted studies by Vadrucci et al., Sorriaux et al., and Gambarini et al. show that the extracted calibration curves for EBT3 film in the Co-60 beam and proton beam are remarkably different [34–36]. Consequently, the employed EBT3 films for proton dose measurements were calibrated by a 60 MeV proton beam at the dose range of 0.5–15 Gy.

All of the irradiated films were stored for 24 hours and then were read using a Microtek 9800XL flatbed scanner (Microtek Inc., CA, USA) and stored in the tagged image file format (Tiff) image files. This scanner is equipped with a transparent media adopter (TMA) which enables the film scanning in

transmission mode [37, 38]. All of the films were scanned in 48-bit RGB mode (16 bits per channel) and the scanning resolution was adjusted to 72 dpi (dot per inch) to maximize the SNR (signal-to-noise ratio) of the film response. It should be mentioned that all image filters and enhancement options were turned off during the film scanning. [32, 38]. All of the scanned films were analyzed in the green channel using an in-house image processing program developed by MATLAB programming software. Due to the high levels of administered doses to the employed EBT3 films, the film response was saturated in the red channel, a fact which forced us to use the green channel during the film dosimetry procedure.

The film response in terms of pixel value (PV) was converted to the net optical density (netOD) by applying the bellow expression [40]:

$$NetOD = \log_{10}(\frac{PV_{before}}{PV_{after}}) \ (1)$$

Where PV_{before} and PV_{after} are the pixel values (PV) of the EBT3 film before and after the exposure, respectively. It is worth mentioning that film handling and maintenance were according to the manufacturer's recommendations as well as the relevant film dosimetry protocol [39].

2.3. Proton beam irradiation

As mentioned previously, to compare the clinical efficacy of proton therapy and brachytherapy using ^{125}I and ^{106}Ru plaques in the treatment of intraocular tumors, the same tumor size and geometry were considered for all three considered treatment modalities. In this regard, an intraocular tumor with a diameter of 12 mm, including a 3 mm margin, was supposed its apex had been located at a 6 mm distance from the eyeball surface. The dimensions and position of the considered tumor inside the eyeball have been illustrated in Fig. 2. Considered OARs have been also indicated in this Figure.

Figure 2.

The proton beam irradiations were performed at CNAO oncological hadron therapy center in Italy. A circular field size with a diameter of 12 mm was used for tumor irradiation with 3 mm lateral margins. The SOBP was created through proton energy modulation between 75.74, 76.63, 77.51, 78.39, 79.26, 80.12, and 80.98 MeV. In addition, an RW3 range shifter with a thickness of 36.1 mm (equivalent to 38 mm thickness of water) was also employed. With this configuration, the plateau region of the SOBP would be equal to 6 mm which is started from the phantom surface. Proton beam delivery was performed using the active beam scanning technique. The tumor region (6 mm depth and 15 mm diameter including lateral margins) was painted by seven successive slices with 10×10 scan spot size in X and Y directions. A 10 Gy proton dose was administered to the tumor (the plateau region of the SOBP) during the irradiation.

For proton beam dosimetry, four film pieces were employed. The first one was aligned along the beam central axis (Z-axis) to measure the percentage depth dose (PDD) distribution and 2D isodose distribution in the X-Z plane. Three remaining film pieces were perpendicular to the central beam axis and were

respectively located at 6, 7, 8, 9, and 10 mm distances from the phantom surface to obtain the relevant transverse dose profiles and 2D isodose distributions in the X-Y plane. Finally, the 3D dose distribution inside the tumor volume was obtained by interpolating/extrapolating the dose values at different points from the measured dose values by all of the employed films (both vertically and horizontally located EBT3 films). Subsequently, the dose-volume histogram (DVH) for both the tumor and surrounding healthy tissues were extracted from the measured dose values.

2.4. ^{106}Ru-based plaque brachytherapy

The size, dimensions, and location of the considered tumor during the ^{106}Ru-based plaque brachytherapy were identical to those taken during the proton irradiation. Given that the proton beam is generally used for the treatment of large intraocular tumors [4, 7], the CGD plaque was selected during the ^{106}Ru-based intraocular brachytherapy because it is more suited for irradiation of large tumor sizes in comparison with commercially available ^{106}Ru plaque types [40].

The CGD plaque has been introduced by Eckert and Ziegler BEBIG GmBH Company. This plaque is made from pure Silver (Ag) and the ^{106}Ru is coated on the inner plaque surface. A 0.1 mm thick Silver-made exit window is located over the radioactive layer, while a 0.7 mm backing material (made from Silver) is also provided for the ^{106}Ru radioactive layer [20, 41]. The available CGD plaque at NOOR Eye hospital in Iran was used for plaque-based brachytherapy.

The CGD plaque is a section of a sphere with a radius of 13 mm. The aperture and height of the plaque are equal to 22.3 mm and 6.1 mm (it should be noted that these dimensions are identical to those of the semispherical part of the employed eyeball phantom). A schematic view of the CGD plaque has been shown in Fig. 3.

Figure 3.

Just as the same as the proton irradiation, four pieces of Gafchromic EBT3 films were also used for CGD plaque dosimetry. The first one was employed for PDD and 2D isodose distribution in the X-Z plane, while the rest films were positioned at 6, 7, 8, 9, and 10 mm distances from the eyeball surface (perpendicular to Z-axis) for measuring the transverse dose profiles, 2D isodose distributions in the X-Y plane, as well as the 3D dose distribution and subsequent DVH data. It should be mentioned that the real prescribed dose to the tumor apex in clinical practice is usually equal to 100 Gy [12, 18, 42].

Nevertheless, it was not possible to administer such large radiation doses to the employed films because of both time limitation and saturation of the film response at very high doses of radiation which occurred at distances close to the eyeball surface. As a result, the radiation dose of 30 Gy was considered at the eyeball surface for this treatment modality to avoid the saturation of the film response.

2.5. ^{125}I-based plaque brachytherapy

Irseed-125 ^{125}I brachytherapy seeds were employed for gamma-based brachytherapy [43, 44]. The irseed-125 model is similar to the 6711 seed model except for the physical and active lengths with are respectively equal to 4.7 mm and 3.2 mm in the case of the irseed-125 model, while these values are equal to 4.6 mm and 3 mm for 6711 ^{125}I brachytherapy seed model [43, 45] The irradiation setup and tumor location were the same as considered for proton therapy and ^{106}Ru-based plaque brachytherapy. The eye plaque of COMS (collaborative ocular melanoma study) design was used for holding and arrangement of employed seed during the eyeball irradiation. This plaque is manufactured with different apertures of 12 to 20 mm with 2 mm steps [46, 47]. The COMS plaque with a 20 mm aperture was employed in the current study. The plaque body is made of a gold alloy with a density of 15.8 g/cm^3. The contributing constituents in gold alloy include Au, Ag, Cu, and Pd with a mass percent of 77%, 14%, 8%, and 1%, respectively. COMS 20-mm has 24 locations for seed insertion and arrangement. According to the Knutsen et al. study [2, 47, 48], the three central locations of the COMS plaque were activated during the intraocular tumor irradiation and other locations were left empty (without seed insertion). The same film dosimetry procedure as followed in the case of the proton beam and ^{106}Ru CGD plaque was considered during the dosimetric measurements in the case of ^{125}I COMS plaque and relevant dosimetric data including PDD data, transverse dose profiles, 2D and 3D dose distributions, as well as the DVH diagram were accordingly extracted from the measured dose values. The schematic diagram of seed arrangement inside the employed COMS plaque from the concave view has been illustrated in Fig. 4.

Figure 4.

3. Results

The PDD data relevant to the proton beam, COMS, and CGD brachytherapy plaques have been shown in Fig. 5. It should be noted that the presented PDD values have been normalized to the received dose by the 6 mm depth from the eyeball surface.

Figure 5.

The measured 2D isodose distributions in the X-Z plane for the proton beam, COMS plaque, as well as CGD plaque have been shown in Fig. 6. For more clarification about how the isodose distribution will cover the target volume and surrounding healthy tissues inside the eyeball, the actual anatomy of the eyeball has been also appended to Fig. 6.

Figure 6.

The transverse dose profiles (perpendicular to the clinical axis) related to the proton beam, COMS plaque, and CGD plaque have been depicted in Fig. 7. Due to the desirable symmetry of the proton radiation field, the transverse dose profiles for the proton beam have been only reported on Y-axis, while the obtained data along both X-axis and Y-axis has been presented for COMS and CGD plaques. As mentioned previously, the reported dose profiles have been measured at the depths of 6, 7, 8, 9, and 10 mm from the

eyeball surface. Here, the relative doses which have been normalized to the tumor apex (6 mm actual tumor) dose are also reported for proton beam, COMS, and CGD plaques.

Figure 7.

The measured 2D isodose distributions in the X-Y plane for proton beam, COMS, and CGD plaques have been illustrated in Fig. 8. The reported data belongs to the depth of 6 mm from the eyeball surface.

Figure 8.

The obtained 3D isodose distributions inside the tumor volume for each considered radiotherapy technique have been shown in Fig. 9. It should be mentioned again that the 3D dose data were acquired through interpolating/extrapolating the measured dose values by the transversely and vertically located EBT3 films.

Figure 9.

The integral DVH data relevant to the proton beam, COMS, and CGD brachytherapy plaques have been shown in Fig. 10. It should be noted that the reported data has been extracted from the measured 3D isodose distributions in Fig. 9. The illustrated DVH results are relevant to both tumor volume as well as the surrounding healthy tissues including the sclera, choroid, retina, ciliary body, eye lens, vitreous humor, iris, optic nerve, optic disc, macula, and cornea which have been schematically illustrated in Fig. 2.

Figure 10.

The ordinate in Fig. 10 shows the relative volume (%), while the abscissa indicates the percentage dose with respect to the received dose by the tumor apex. For example, V_{60} shows the volume percentage which receives at least 60% of the delivered dose to the tumor apex. It should be noted that the abscissa for COMS and CGD plaques has been extended to much greater values than the proton beam. This issue is due to the large received dose to the regions which are proximal to the plaque surface. Therefore, to provide a better comparison between the obtained DVH data for the three techniques understudy, especially for the healthy organs which receive lower dose values, the DVH data have been also reported up to 100% relative dose value on the horizontal axis.

4. Discussion

Comparing the drawn PDD data in Fig. 5 reveals that a steep dose gradient along the central axis would be observed in the case of ^{125}I and ^{106}Ru brachytherapy plaques, while a rather uniform dose distribution would be found along the Z-axis (along the tumor depth) in the case of the proton beam. For example, by increasing the distance from the surface to 6 mm away (the spatial range at which the tumor is deeply distributed), the PDD value will respectively reduce by about 78%, 76%, and 7% for COMS plaque, CGD plaque, and proton beam. The main reason for the observed steep dose gradient for COMS and CGD plaques is the relatively low energy nature of the emitted radiations from ^{125}I and ^{106}Ru radioactive

sources. In this regard, the maximum electron energy which is emitted during the different beta-minus decay channels of ^{106}Ru is about 3.5 MeV [49]. The mean emitted photon energy from ^{125}I radioactive material is also about 28.37 keV [50]. This finding explicitly indicates that a more uniform dose distribution inside the target volume and along the Z-axis would be obtained when the proton beam is employed for irradiation of the intraocular malignancies in comparison with both photon and electron beam (^{125}I and ^{106}Ru brachytherapy plaques, respectively). On the other hand, for regions that are located behind the tumor volume (depths beyond 6 mm in the current study), the dose fall-off along the central axis for the proton beam is more appreciable in comparison with both CGD plaque and COMS plaque. For example, with moving from 6 mm to 10 mm depth, the PDD data decrements by about 95%, 90%, and 59% for proton beam, CGD plaque, and COMS plaque, respectively). Although the mean energy of the emitted photons from ^{125}I is quite low, some numbers of photons will always pass the tumor and can consequently increase the received dose along the central axis at the regions which are located behind the tumor volume.

For regions before the tumor volume (such as sclera, as shown in Fig. 2), the dose during the plaque-based brachytherapy would be several times higher than the administered dose by the proton beam. In this regard, the COMS plaque would deliver the maximum dose to the overlaying regions (i.e., the presented PDD data in Fig. 5 indicates that the PDD value at the surface would be about 462%, 419%, and 108% for COMS plaque, CGD plaque, and proton beam, correspondingly).

As illustrated by Fig. 6, the lateral spreading of the isodose curves is more obvious in the case of the CGD brachytherapy plaque with respect to other studied modalities. The main reason for this issue is the multiple electrons scattering into the lateral regions, especially at lower energies, which can finally lead to the spreading of the isodose lines to the lateral regions. The special design of the CGD plaque which contains a large radioactive aperture with a 20.3 mm diameter can also contribute to this finding. This lateral spreading in isodose lines may lead to the overexposure of the laterally distributed OARs which are located in close vicinity of the tumor volume such as the ciliary body. On the other hand, the less lateral spreading of the isodose curve is found in the case of ^{125}I COMS plaque, according to Fig. 6, which can reduce the administered dose to the lateral region adjacent to the tumor volume. The minimum lateral spreading was found for the proton beam, as demonstrated in Fig. 6. Because of high mass, the proton beam will experience small deviations from its original direction and accordingly, it can be expected that a negligible lateral spreading would be observed for the relevant isodose curve to the proton beam. Therefore, the proton beam can minimize the received dose by laterally-distributed healthy tissues among the treatment modalities understudy and consequently more efficiently spare such OARs.

As demonstrated in Fig. 6, the most desirable dose uniformity within the tumor region is relevant to the proton beam. This fact is mainly linked to the much more uniform depth dose distribution of the proton beam in comparison with the considered brachytherapy plaques of CGD and COMS. In this regard, the tumor volume falls within the SOBP region for the proton beam, while in the case of COMS and CGD plaques, the tumor region lies within a descending part of the PDD curve with a very steep dose gradient (as shown in Fig. 5).

Comparison among the obtained transverse dose profiles for the proton beam, COMS, and CGD plaque in Fig. 7 clearly shows that the uniformity of the lateral dose distribution at all studied depths is more remarkable for the proton beam. This fact is mainly linked to the uniform dose painting by applying the active beam scanning technique for the proton dose delivery system.

On the other hand, a completely non-uniform lateral dose distribution would be observed for the COMS and CGD plaques. In this regard, substantial horns are found at the filed edges in both X and Y dimensions for the CGD plaque. Increasing the off-axis distance from the plaque central axis decreases the distance between the intended dosimetry point and the inner plaque surface. Consequently, it can be expected that a more radiation dose would be received at these laterally located points and therefore, such horns will have appeared in the measured transverse dose profiles on both X-axis and Y-axis. The other potential reasons for such horns can be the non-uniform coating of the ^{106}Ru radioactive layer upon the inner surface of the employed CGD plaque as well as the multiple electrons scattering into the lateral regions. The presence of these horns can remarkably contribute to the overexposure of the laterally distributed healthy tissues when the CGD plaque is applied for treatment. Besides, these lateral dose non-uniformities can disrupt the homogeneity of the dose distribution within the target volume.

The measured transverse dose profiles for the COMS plaque show a peak at the mid-region in both X and Y directions for all considered depths. Then, the dose value sharply reduces with moving away from the central region. Such behavior can be justified by the arrangement of ^{125}I brachytherapy seeds loaded within the COMS plaque. As shown in Fig. 4, the radioactive ^{125}I seeds are located at the central part of the COMS plaque and therefore it can be expected that the corresponding regions inside the phantom will absorb the maximum dose value. On the other hand, the peripheral regions of COMS plaque are empty. Therefore, much lower dose values would be received to the corresponding lateral distances inside the phantom.

More uniform dose distribution for the proton beam concerning that of the COMS and CGD plaque is also obvious when the reader compares the relevant 2D isodose distributions to the considered intraocular tumor treatment techniques in Fig. 8. Furthermore, the COMS plaque also shows better dose uniformity with respect to the CGD plaque the in X-Y plane. The presence of the horns in measured dose profiles for CGD plaque can affect the uniformity of the 2D isodose distributions in the X-Y plane. As indicated in Fig. 8, some hot spots have been formed at the lateral regions which are associated with the presence of the horns in measured transverse dose profiles for CGD plaque.

The more uniform coverage of the tumor volume by the proton beam with respect to the COMS plaque and CGD plaque is evident from Fig. 9, a fact that was previously discussed in detail. Besides, the remarkable lateral spreading of the relevant isodose curves to the CGD plaque with respect to the proton beam and COMS plaque is also obvious from the illustrated results in Fig. 9. This issue was also fully explained in previous sections.

According to a more uniform dose distribution inside the tumor region during the proton beam irradiation, it can be expected that the relevant DVH to the tumor volume shows a wide plateau region, as declared in Fig. 10. On the other hand, non-uniform dose delivery to the tumor region through applying the COMS and CGD plaque results in a descending DVH for tumor volume with a very short plateau region. The reported DVH data in Fig. 10 also demonstrates that dose uniformity inside the tumor volume is superior in the case of COMS plaque with respect to the CGD plaque. This fact was also confirmed by the obtained 3D isodose distribution data in Fig. 9. Therefore, using the proton beam and electron beam respectively results in the best and the worst performance viewpoint on the dose uniformity inside the target volume.

The demonstrated data in Fig. 10 indicates that the proton beam can more efficiently spare the distributed OARs around the tumor volume in comparison with the COMS and CGD brachytherapy plaques. This issue is mainly attributed to the minimum lateral spreading of the proton beam during the passage from the eyeball which was discussed earlier.

As illustrated by Fig. 10, healthy organs such as the eye lens, optic disc, optic nerve, and macula can be better spared using the CGD plaque rather than the COMS one. This finding can be well justified by the presented results in Fig. 6. As shown in Fig. 6, the extension of isodose lines within the above-mentioned OARs is lower in the case of CGD plaque with respect to the COMS one. Viewpoint to the fact that the eye lens, optic disc, and optic nerve are sensitive organs, using the CGD plaque would be preferred to the COMS plaque, provided that sparing other healthy organs during the radiotherapy is not to be considered.

On the other hand, healthy organs such as the sclera, choroid, retina, ciliary body, cornea, iris, and vitreous humor are better spared using the COMS plaque in comparison with the CGD one. This finding can be also justified by the presented results in Fig. 6. The spreading of the isodose lines within the above-mentioned OARs is lower in the case of COMS plaque (refer to Fig. 6) and therefore, it can be deduced that lower dose values would be received to these healthy organs when the CGD plaque is substituted by the COMS plaque.

5. Conclusions

The clinical efficacy of the proton beam therapy and plaque-based brachytherapy using COMS and CGD plaques in the treatment of the intraocular tumors were practically measured and compared through the Gafchromic film dosimetry approach in terms of the received dose by the tumor volume as well as the surrounding healthy tissues.

Our findings demonstrate that the proton beam irradiation can result in a more uniform dose distribution inside the target volume, a fact that can lead to an improved tumor control probability (TCP) during the treatment. Furthermore, the intraocular proton therapy can better spare the laterally distributed OARs with respect to both ^{125}I and ^{106}Ru plaque-based brachytherapy techniques. Comparing the obtained DVH data for COMS and CGD plaque also demonstrates that the COMS plaques generally show a better performance regarding the dose uniformity inside the target volume as well as the received dose by the

surrounding healthy tissues. Nevertheless, the eye lens, optic nerve, optic disc, and macula are better saved when the CGD plaque is employed for brachytherapy. Therefore, based on the importance of the OAR which should be spared, the COMS or CGD plaque can be selected for radiotherapy.

From the results, it can be finally concluded that using the proton beam would be preferred to the photon and electron beam for eyeball irradiation, provided that the radiotherapy department is equipped with hadron therapy technology. Otherwise, using the photon beam can lead to superior clinical efficacy concerning the electron beam in the radiotherapy of intraocular tumors.

Declarations

Funding

The authors declare that no funds, grants, or other support were received during the preparation of this manuscript.

Acknowledgment

The authors wish to thank Prof. Roberto Cirio for his very kind support during the proton beam irradiations.

Competing Interests

The authors have no relevant financial or non-financial interests to disclose.

Author Contributions

All authors contributed to the study conception and design. Material preparation, data collection and analysis were performed by [Taha Eidi], [Seyed Mahmoud Reza Aghamiri] and [Hamid Reza Baghani]. The first draft of the manuscript was written by [Taha Eidi and Hamid Reza Baghani] and all authors commented on previous versions of the manuscript. All authors read and approved the final manuscript.

Compliance with Ethical Standards

Conflict of Interest: Author [Taha Eidi] declares that he has no conflict of interest. Author [Seyed Mahmoud Reza Aghamiri] declares that he has no conflict of interest. Author [Hamid Reza Baghani] declares that he has no conflict of interest.

Ethical approval: This article does not contain any studies with human participants or animals performed by any of the authors.

Informed consent: None declared.

References

1. Lutz J-M, Cree IA, Foss AJ (1999) Risk factors for intraocular melanoma and occupational exposure. Br J Ophthalmol 83(10):1190–1193
2. Russo I, Levy-Gabriel C, Dupont A, Lumbroso-Le Rouic L, Cassoux N, Desjardins L, Bertozzi AI, Coze C, Doz F, Savignoni A (2021) Prospective phase II study of children affected by bilateral intraocular retinoblastoma with macular involvement of both eyes or in the only preserved eye. Macular tumor control, eye preservation rate, and visual outcome. Pediatr Blood & Cancer 68(1):e28721
3. van Beek JG, Ramdas WD, Angi M, van Rij CM, Naus NC, Kacperek A et al (2021) Local tumour control and radiation side effects for fractionated stereotactic photon beam radiotherapy compared to proton beam radiotherapy in uveal melanoma. Radiother Oncol 157:219–224
4. Eidi T, Aghamiri SMR, Jaberi R, Baghani HR (2021) On measuring the 3D dose distribution for notched and circular Ru-106 plaque shapes through Gafchromic film dosimetry approach.Radiat Phys Chem,109792
5. Espensen CA, Kiilgaard JF, Appelt AL, Fog LS, Herault J, Maschi C et al (2021) Dose-response and normal tissue complication probabilities after proton therapy for choroidal melanoma. Ophthalmolo 128(1):152–161
6. Thornton S, Coupland SE, Heimann H, Hussain R, Groenewald C, Kacperek A et al (2020) Effects of plaque brachytherapy and proton beam radiotherapy on prognostic testing: a comparison of uveal melanoma genotyped by microsatellite analysis. Br J Ophthalmol 104(10):1462–1466
7. Tseng VL, Coleman AL, Zhang Z-F, McCannel TA (2016) Complications from plaque versus proton beam therapy for choroidal melanoma: a qualitative systematic review. J Cancer Ther 7(3):169–185
8. Mourtada F, Koch N, Newhauser W (2005) 106Ru/106Rh plaque and proton radiotherapy for ocular melanoma: a comparative dosimetric study. Radiat Prot Dosimetry 116(1–4 Pt 2):454–460
9. Devlin PM (2015) Brachytherapy: applications and techniques. Springer Publishing Company
10. Deufel CL, Culberson WS, Rivard MJ, Mourtada F (2021) Brachytherapy dosimetry. Radiation Therapy Dosimetry: A Practical Handbook. CRC press;, pp 230–252
11. Force T, Simpson ER, Gallie B, Laperrierre N, Beiki-Ardakani A, Kivelä T et al (2014) The American Brachytherapy Society consensus guidelines for plaque brachytherapy of uveal melanoma and retinoblastoma. Brachytherapy 13(1):1–14
12. Pagulayan C, Heng SM, Corde S (2019) Dosimetric validation of the Theragenics AgX-100® I-125 seed for ROPES eye plaque brachytherapy. Australas Phys Eng Sci Med 42(2):599–609
13. Bakshi A, Vandana S, Selvam TP, Rama P, Manolkar R, Chougaonkar M et al (2014) Study on the characteristics of indigenously developed 106Ru/106Rh source. Radiat Meas 64:23–28
14. Ghassemi F, Sheibani S, Arjmand M, Poorbaygi H, Kouhestani E, Sabour S et al (2020) Comparison of iodide-125 and ruthenium-106 brachytherapy in the treatment of choroidal melanomas. Clin Ophthalmol (Auckland NZ) 14:339
15. Wilkinson D, Kolar M, Fleming P, Singh A (2008) Dosimetric comparison of 106Ru and 125I plaques for treatment of shallow (≤ 5 mm) choroidal melanoma lesions. Br j radiol 81(970):784–789

16. Chappelow A, Singh A, Wilkinson D, Kolar M, Fleming P (2007) Comparison of Radiation Dosage to Ocular Structures With Ru-106 and I-125 Plaques for Choroidal Melanoma. IOVS 48(13):5235
17. Jiang P, Purtskhvanidze K, Kandzia G, Neumann D, Luetzen U, Siebert F-A et al (2020) 106 Ruthenium eye plaque brachytherapy in the management of medium sized uveal melanoma. Radiat Oncol 15(1):1–6
18. Kirov AS, Piao J, Mathur N, Miller T, Devic S, Trichter S et al (2005) The three-dimensional scintillation dosimetry method: test for a 106Ru eye plaque applicator. Phys Med Bio 50(13):3063
19. Eidi R, Aghamiri SM, Sheibani S, Jaberi R, Pourbeigi H, Mashayekhi Galatoiyeh M et al (2014) Silastic Thickness Optimization in Uveal Melanoma Brachytherapy by Monte Carlo Method. Iran J Med Phys 11(1):175–181
20. Thomson RM, Furutani KM, Kaulich TW, Mourtada F, Rivard MJ, Soares CG et al (2020) AAPM recommendations on medical physics practices for ocular plaque brachytherapy: Report of task group 221. Med Phys 47(5):e92–e124
21. Ciocca M, Magro G, Mastella E, Mairani A, Mirandola A, Molinelli S et al (2019) Design and commissioning of the non-dedicated scanning proton beamline for ocular treatment at the synchrotron-based CNAO facility. Med Phys 46(4):1852–1862
22. Piersimoni P, Rimoldi A, Riccardi C, Pirola M, Molinelli S, Ciocca M (2015) Optimization of a general-purpose, actively scanned proton beamline for ocular treatments: Geant4 simulations. J Appl Clin Med phys 16(2):261–278
23. Lin AJ, Rao YJ, Acharya S, Schwarz J, Rao PK, Grigsby P (2017) Patterns of care and outcomes of proton and eye plaque brachytherapy for uveal melanoma: review of the National Cancer Database. Brachytherapy 16(6):1225–1231
24. Cirrone G, Cuttone G, Lojacono P, Nigro SL, Mongelli V, Patti I et al (2004) A 62-MeV proton beam for the treatment of ocular melanoma at Laboratori Nazionali del Sud-INFN. IEEE Trans Nucl Sci 51(3):860–865
25. Kato T (2019) Current Status of Dosimetry Tools for Clinical Proton Beams. REM 8:56–69
26. Rossi S (2011) The status of CNAO. EPJ Plus 126(8):1–39
27. Van der Walt M, Crabtree T, Albantow C (2019) PLA as a suitable 3D printing thermoplastic for use in external beam radiotherapy. Australas Phys Eng Sci Med 42(4):1165–1176
28. Diamantopoulos S, Kantemiris I, Patatoukas G, Dilvoi M, Efstathopoulos E, Kouloulias V et al (2018) Theoretical and experimental determination of scaling factors in electron dosimetry for 3D-printed polylactic acid. Med Phys 45(4):1708–1714
29. Devic S (2011) Radiochromic film dosimetry: past, present, and future. Phys Med 27(3):122–134
30. Baghani HR, Aghamiri SMR, Mahdavi SR, Robatjazi M, Zadeh AR, Akbari ME et al (2015) Dosimetric evaluation of Gafchromic EBT2 film for breast intraoperative electron radiotherapy verification. Phys Med 31(1):37–42

31. Vaiano P, Consales M, Casolaro P, Campajola L, Fienga F, Di Capua F et al (2019) A novel method for EBT3 Gafchromic films read-out at high dose levels. Phys Med 61:77–84
32. Marroquin EYL, Herrera Gonzalez JA, Camacho Lopez MA, Barajas JEV, García-Garduño OA (2016) Evaluation of the uncertainty in an EBT3 film dosimetry system utilizing net optical density. J Appl Clin Med Phys 17(5):466–481
33. Sanchez-Parcerisa D, Sanz-García I, Ibáñez P, España S, Espinosa A, Gutiérrez-Neira C et al (2021) Radiochromic film dosimetry for protons up to 10 MeV with EBT2, EBT3 and unlaminated EBT3 films. Phys Med Bio 66(11):115006
34. Gambarini G, Bettega D, Camoni G, Barzon G, Bettinelli L, Giove D et al (2019) Development of a procedure for quenching-effect correction in images of absorbed dose from protons or carbon ions acquired with Gafchromic EBT3 films. Radiat Phys Chem 155:138–145
35. Vadrucci M, Esposito G, Ronsivalle C, Cherubini R, Marracino F, Montereali R et al (2015) Calibration of GafChromic EBT3 for absorbed dose measurements in 5 MeV proton beam and 60Co γ-rays. Med Phys 42(8):4678–4684
36. Sorriaux J, Kacperek A, Rossomme S, Lee JA, Bertrand D, Vynckier S et al (2013) Evaluation of Gafchromic® EBT3 films characteristics in therapy photon, electron and proton beams. Phys Med 29(6):599–606
37. Carrasco M, Perucha M, Luis F, Baeza M, Herrador M (2013) A comparison between radiochromic EBT2 film model and its predecessor EBT film model. Phys Med 29(4):412–422
38. Micke A, Lewis DF, Yu X (2011) Multichannel film dosimetry with nonuniformity correction. Med Phys 38(5):2523–2534
39. Niroomand-Rad A, Chiu-Tsao S-T, Grams MP, Lewis DF, Soares CG, Van Battum LJ et al (2020) Report of AAPM task group 235 radiochromic film dosimetry: an update to TG-55. Med Phys 47(12):5986–6025
40. Marconi DG, de Castro DG, Rebouças LM, Gil GOB, Fogaroli RC, Maia MAC et al (2013) Tumor control, eye preservation, and visual outcomes of ruthenium plaque brachytherapy for choroidal melanoma. Brachytherapy 12(3):235–239
41. Brualla L, Zaragoza FJ, Sauerwein W (2015) Monte Carlo simulation of the treatment of eye tumors with 106Ru plaques: a study on maximum tumor height and eccentric placement. Ocul Oncol Pathol 1(1):2–12
42. Fili M, Astrahan M, Stålhammar G (2021) Long-term outcomes after enucleation or plaque brachytherapy of choroidal melanomas touching the optic disc. Brachytherapy
43. Lohrabian V, Sheibani S, Aghamiri MR, Ghozati B, Pourbeigi H, Baghani HR (2013) Determination of dosimetric characteristics of irseed 125i brachytherapy source. Iran J Med Phys 10(2):109–117
44. Taherparvar P, Fardi Z (2021) Development of GATE Monte Carlo Code for Simulation and Dosimetry of New I-125 Seeds in Eye Plaque Brachytherapy. Nucl Med Mol Imaging 55(2):86–95
45. Baghani H, Lohrabian V, Aghamiri MR, Robatjazi M (2016) Monte Carlo determination of dosimetric parameters of a new 125I brachytherapy source according to AAPM TG-43 (U1) protocol. Arch. Iran

Med 19 186 – 91.

46. Chiu-Tsao ST, Astrahan MA, Finger PT, Followill DS, Meigooni AS, Melhus CS et al (2012) Dosimetry of 125I and 103Pd COMS eye plaques for intraocular tumors: Report of Task Group 129 by the AAPM and ABS. Med Phys 39(10):6161–6184
47. Zabihzadeh M, Rezaee H, Hosseini SM, Feghhi M, Danyaei A, Hoseini-Ghahfarokhi M (2019) Improvement of dose distribution in ocular brachytherapy with 125I seeds 20-mm COMS plaque followed to loading of choroidal tumor by gold nanoparticles. J Cancer Res Ther 15(3):504
48. Knutsen S, Hafslund R, Monge OR, Valen H, Muren LP, Rekstad BL et al (2001) Dosimetric verification of a dedicated 3D treatment planning system for episcleral plaque therapy. Int J Radiat Oncol Biol Phys 51(4):1159–1166
49. Bakshi A, Shrivastava V, Chattaraj A, Samuel K, Selvam TP, Sapra B et al (2021) Surface dose rate variations in planar and curved geometries of 106Ru/106Rh plaque sources for ocular tumors. Phys Med 89:200–209
50. Rivard MJ, Coursey BM, DeWerd LA, Hanson WF, Saiful Huq M, Ibbott GS et al (2004) Update of AAPM Task Group No. 43 Report: A revised AAPM protocol for brachytherapy dose calculations. Med Phys 31(3):633–674

Figures

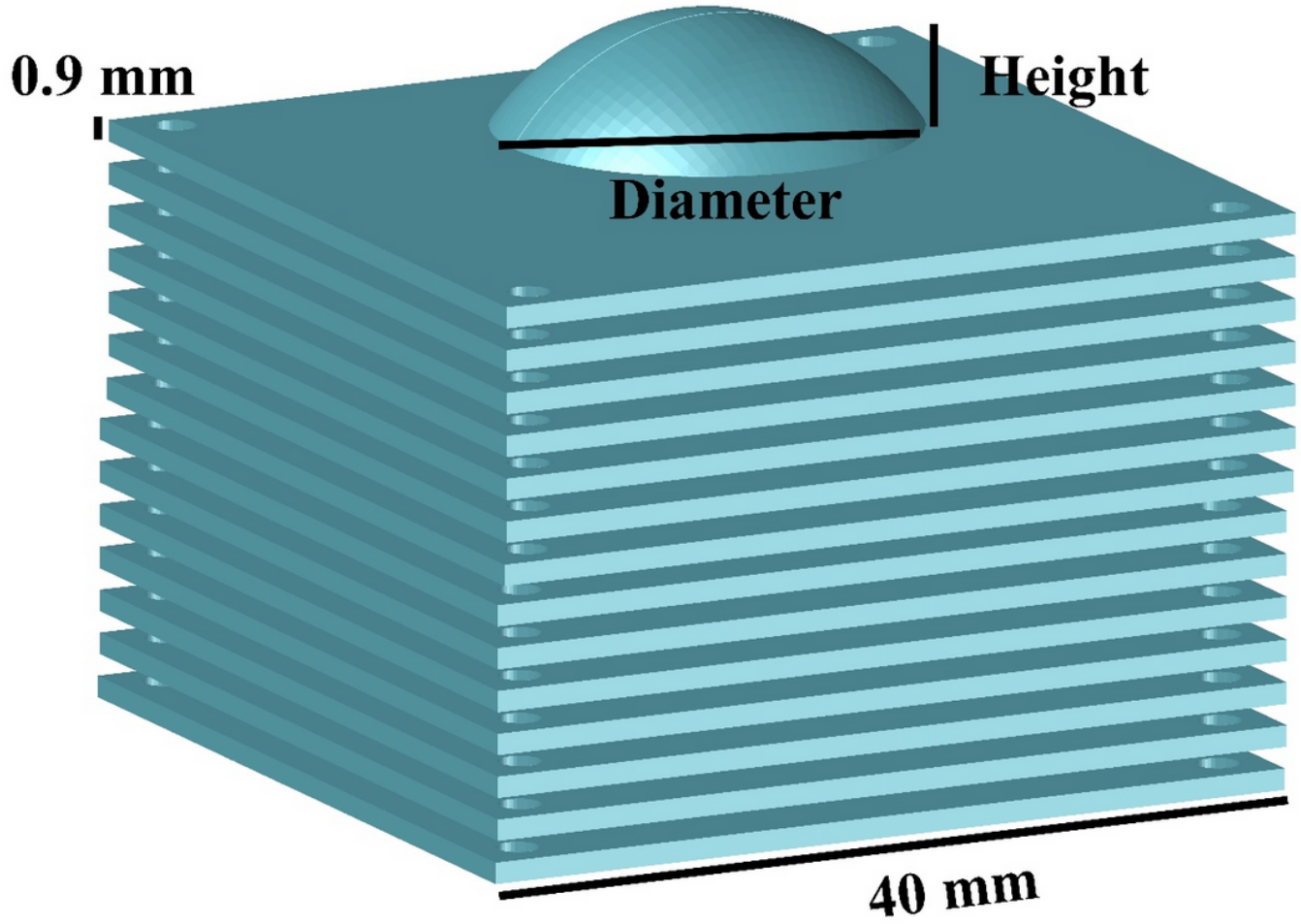

Figure 1

Schematic view of the developed eyeball phantom for radiation dosimetry in the current study.

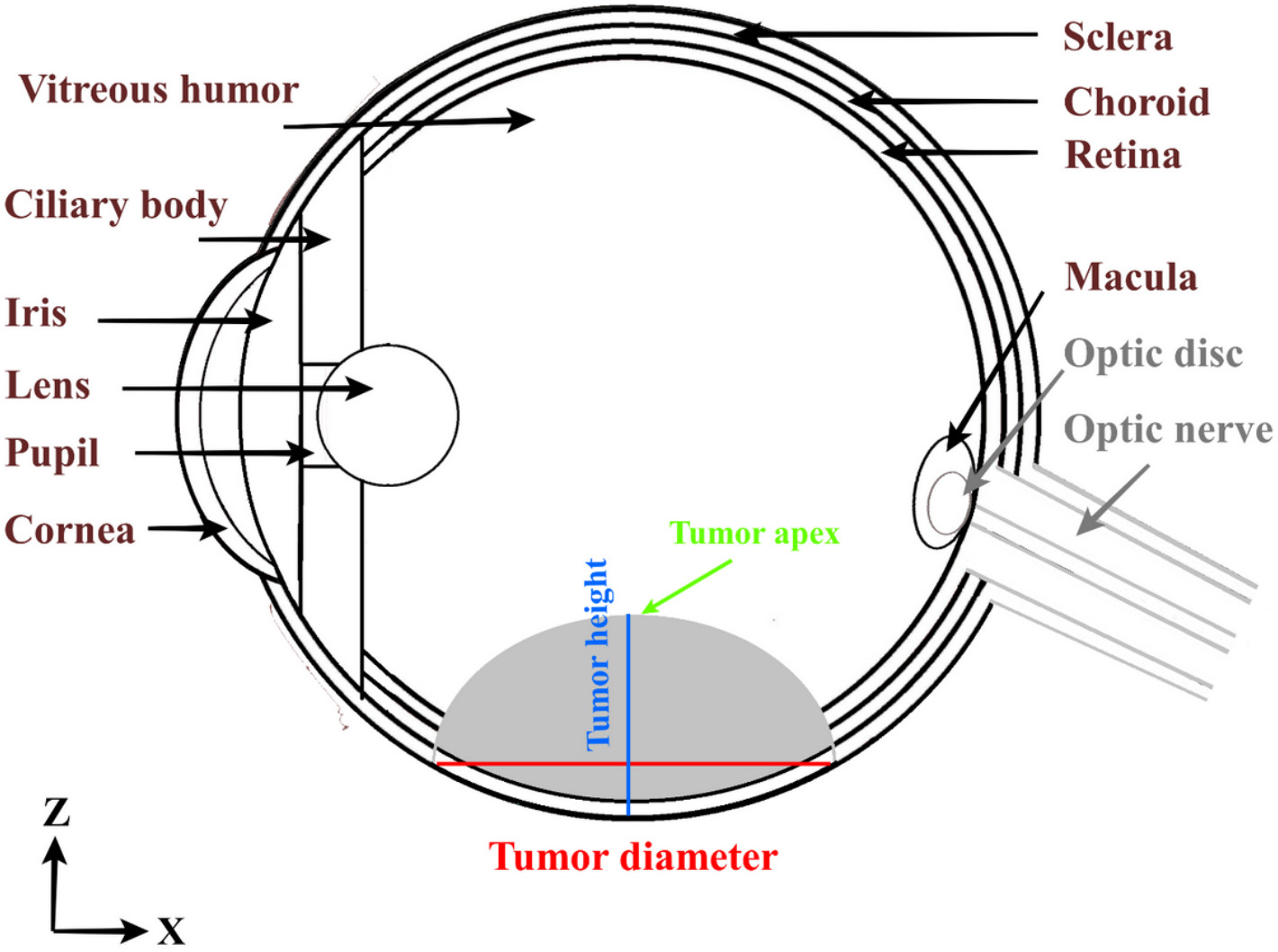

Figure 2

The eyeball anatomy including the considered intraocular tumor as well as the surrounding healthy tissues.

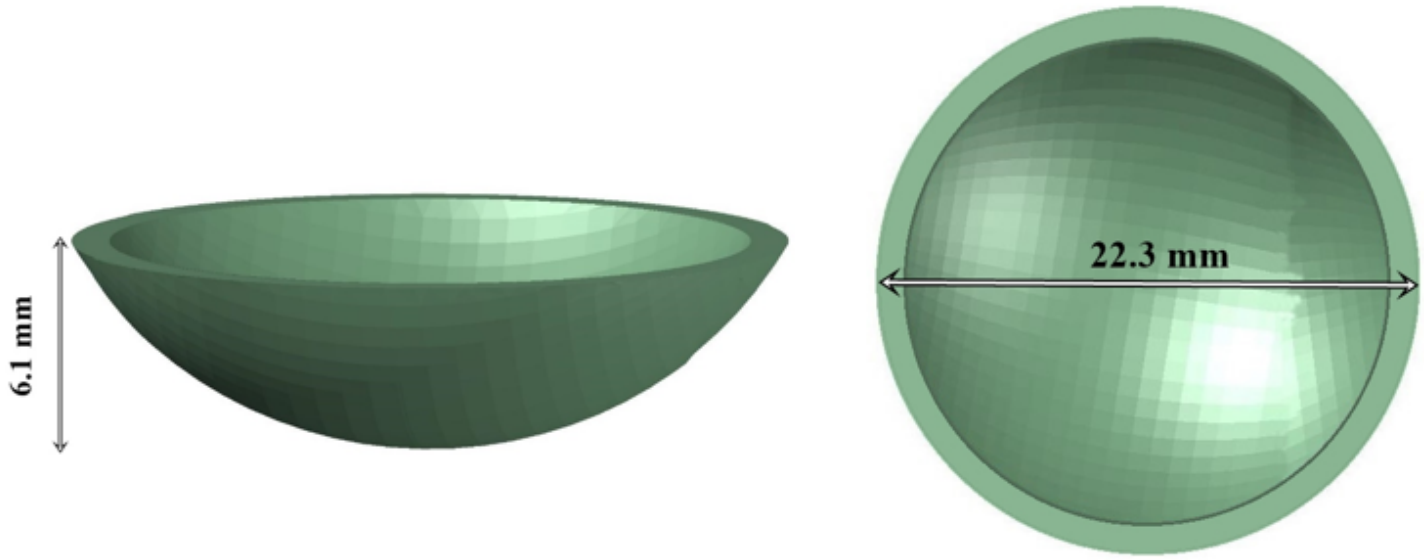

Figure 3

Schematic diagram of the ^{106}Ru CGD plaque for intraocular tumor irradiation. The height (right panel) and diameter (left panel) of the plaque has been illustrated in this Figure.

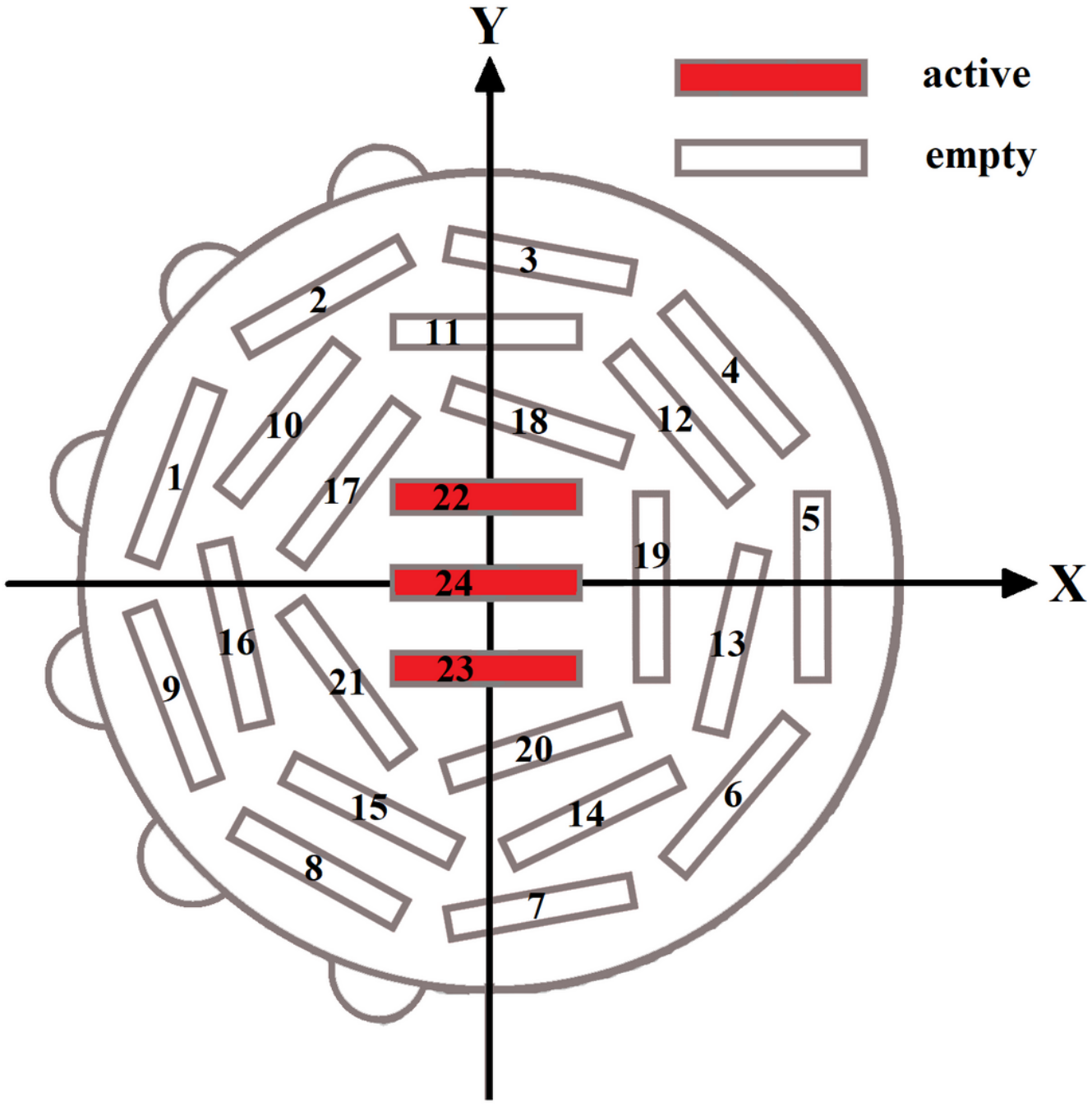

Figure 4

Schematic diagram of loading the COMS plaque with ^{125}I brachytherapy seeds. As demonstrated only three seed places have been activated by ^{125}I seeds (insert numbers of 22, 23, and 24 in the central part of the COMS plaque) and other places have left empty.

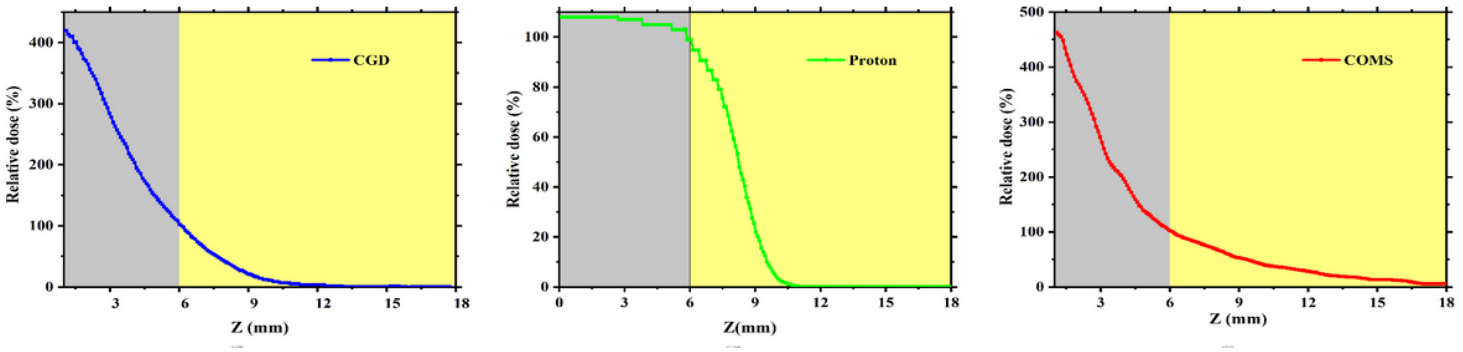

Figure 5

The relative depth dose distribution along the Z-axis for CGD brachytherapy plaque (left panel), proton beam (middle panel) and COMS plaque (right panel). The distribution of the tumor and underlying healthy tissues along the Z-axis have been also illustrated by yellow and turquoise color, respectively.

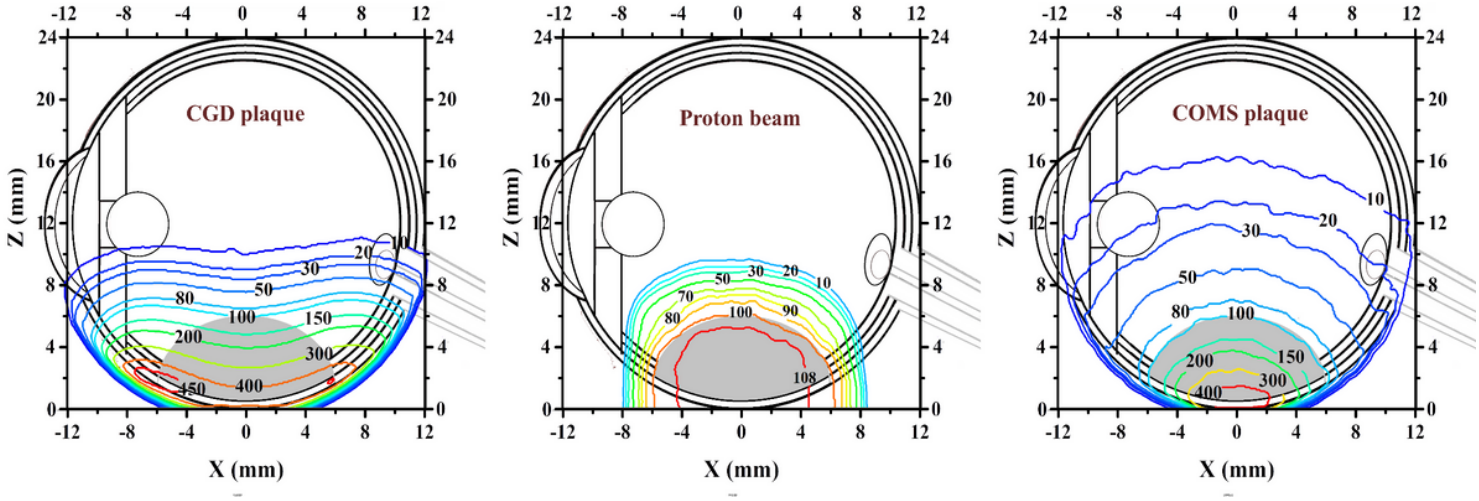

Figure 6

The measured isodose distributions inside the X-Z plane for CGD plaque (left panel), proton beam (middle panel), and COMS plaque (right panel). For more clarification, the eyeball geometry has been also appended to each corresponding panel.

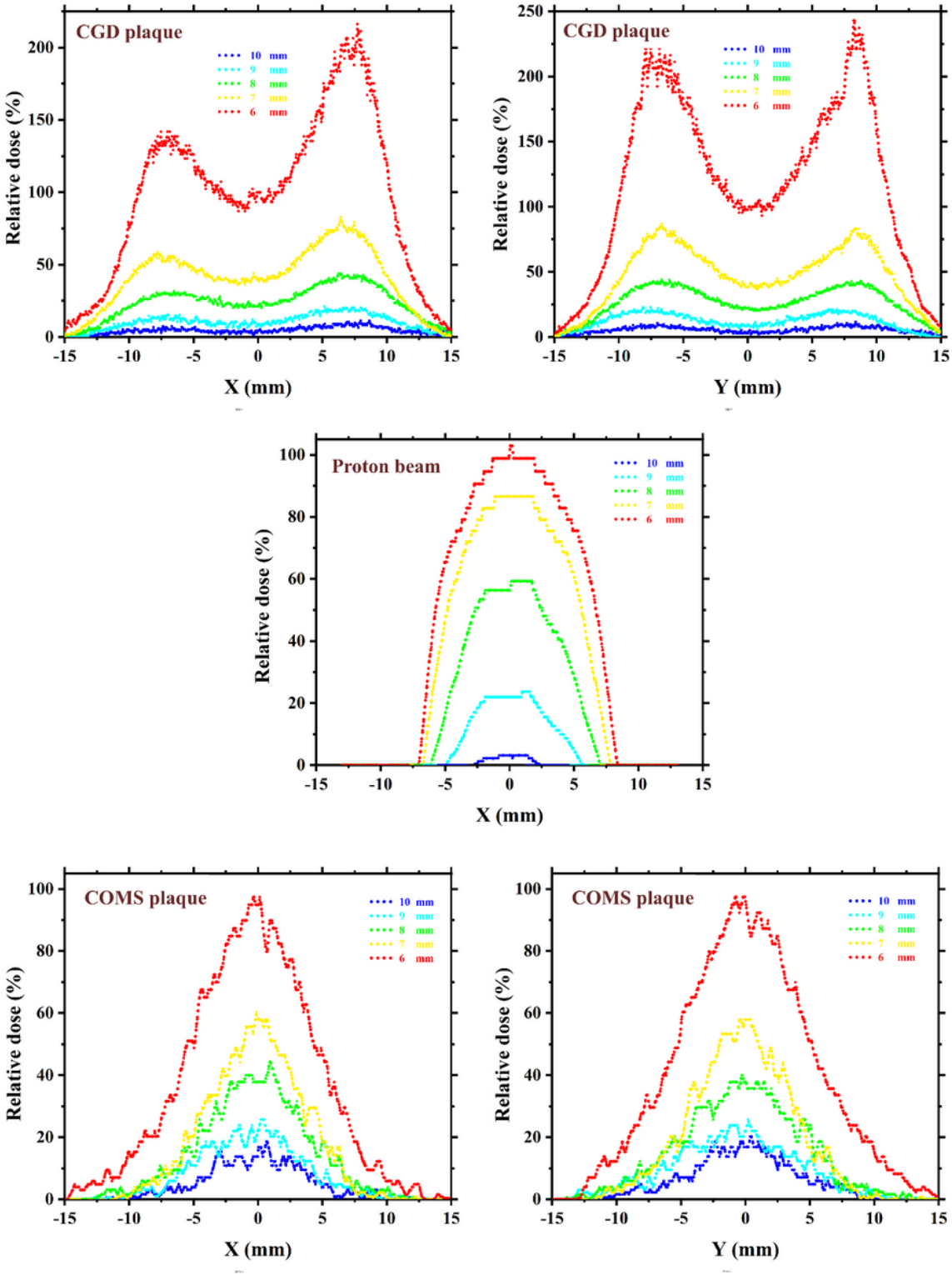

Figure 7

The measured transverse dose profiles along X-axis and Y-axis for CGD plaque (upper panel), proton beam (middle panel), and COMS plaque (lower panel) at different depths of 4, 6, and 8 mm from the eyeball surface. Due to the symmetry in X and Y axes, the relevant transverse dose profiles related to the proton beam have been only depicted along the X-axis.

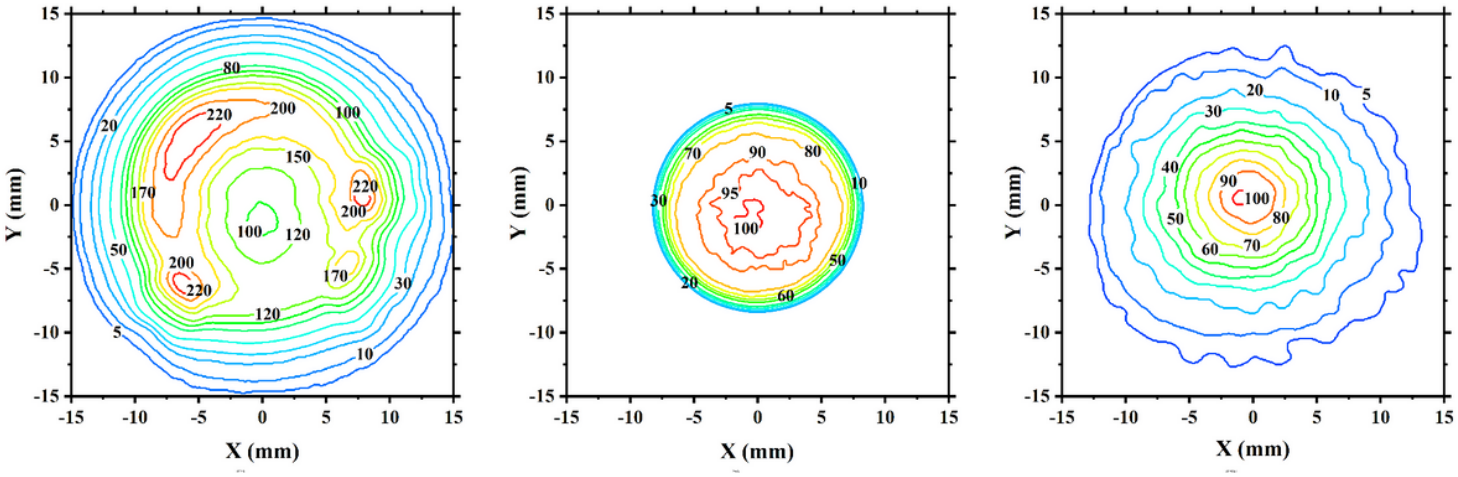

Figure 8

The measured isodose distribution inside the X-Y plane for CGD plaque (left panel), proton beam (middle panel), and COMS plaque (right panel) at the depth of 6 mm from eyeball surface.

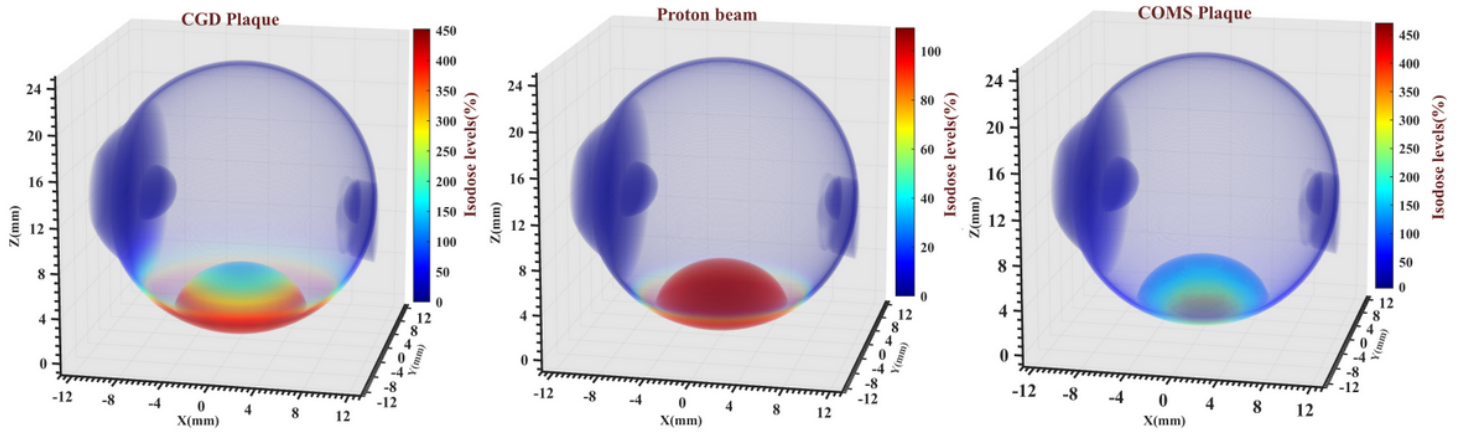

Figure 9

The measured 3D dose distribution for CGD plaque (left panel), proton beam (middle panel), and COMS plaque (right panel).

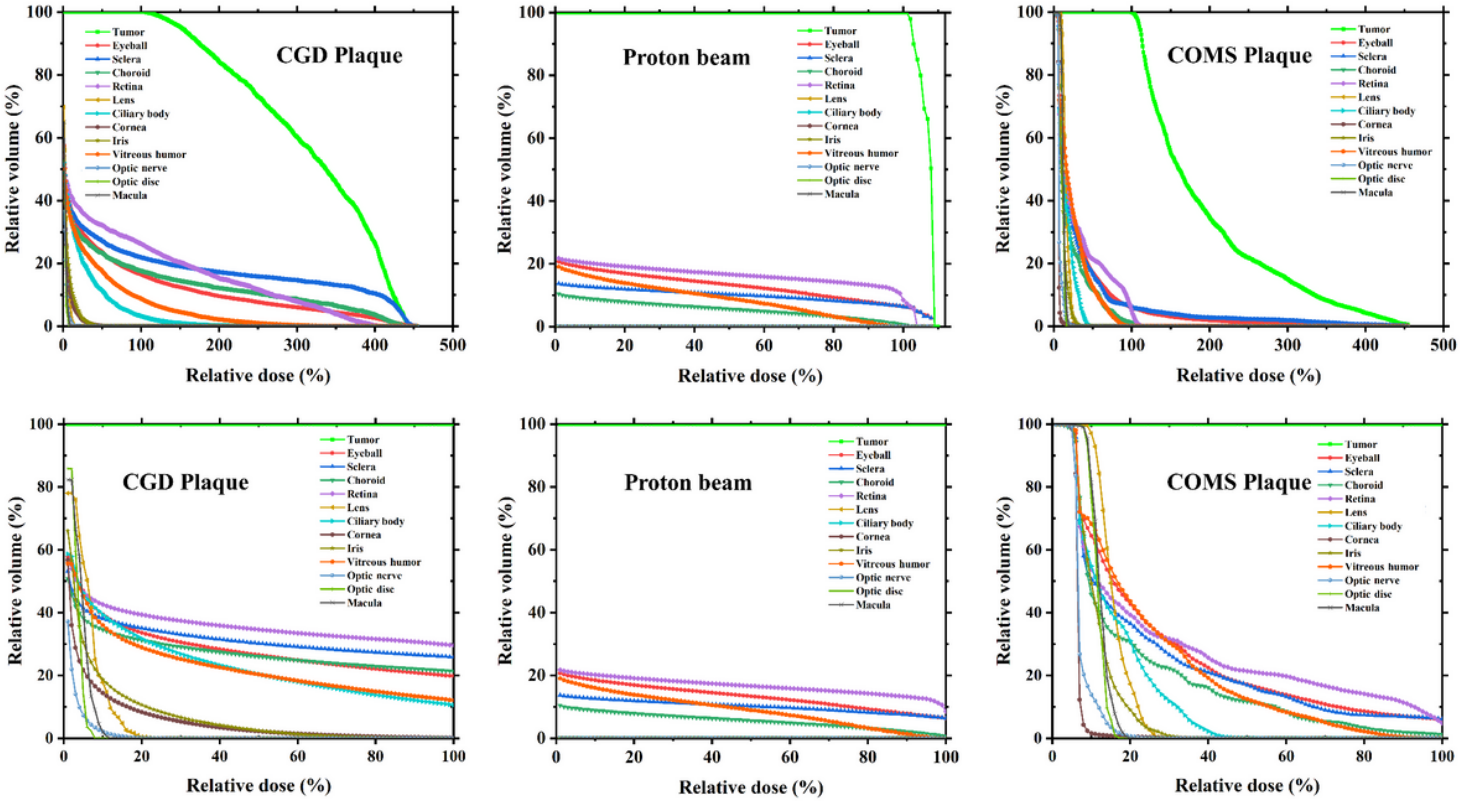

Figure 10

Extracted DVH data relevant to the tumor volume and surrounding healthy tissues for CGD plaque (left panel), proton beam (middle panel), and COMS plaque (right panel). For better comparison, DVH data up to 100% relative dose, on horizontal axis, have been also depicted below each corresponding DVH diagram.